

An origin of narrow extended structure in the interstellar medium: an interstellar contrail created by a fast-moving massive object

KANTA KITAJIMA ^{1,*} AND SHU-ICHIRO INUTSUKA ¹

¹*Department of Physics,
Graduate School of Science,
Nagoya University,
Furo-cho, Chikusa-ku, Nagoya 464-8692, Japan*

(Accepted January 30, 2023)

Submitted to ApJ

ABSTRACT

We investigate the thermal condensation caused by a massive object that passes through the interstellar medium with high velocity, and propose a mechanism for creating a filamentary gaseous object, or interstellar contrail. Our main result shows that a long interstellar contrail can form with a certain parameter; a compact object more massive than $10^4 M_{\odot}$ can make a filament whose length is larger than 100 pc. Observation of interstellar contrails may provide information on the number, masses, and velocities of fast-moving massive objects, and can be a new method for probing invisible gravitating sources such as intermediate-mass black holes.

Keywords: filament, intermediate-mass black hole

1. INTRODUCTION

A sizable fraction of interstellar gas is in approximate thermal equilibrium where heating and cooling are balanced (e.g., [Ferrière 1998](#)). The stable phases are classified as the cold neutral medium (CNM) and the warm neutral medium (WNM) (e.g., [Field et al. 1969](#); [Cox 2005](#)). When a shock wave propagates through such a stable gas, it is compressed by thermal condensation (e.g., [Field 1965](#); [Falle et al. 2020](#)). Supernovae are supposed to be the main cause of those shock waves, and their interactions with the interstellar medium (ISM) have been extensively studied (e.g., [Koyama & Inutsuka 2000, 2002](#); [Audit & Hennebelle 2005](#); [Inoue & Inutsuka 2008, 2009](#); [Kupilas et al. 2021](#)).

We propose that a massive compact object that moves fast creates a filamentary structure (interstellar contrail). This is because by gravitational focusing due to the massive compact object moving fast, a shock wave is driven and thermal condensation occurs. Although it has been suggested that trajectories of celestial objects create structure in interstellar space (e.g., [Wallin et al. 1996](#); [Martinez-Medina et al. 2016](#); [Li & Shi 2021](#)), quantitative analysis of the resultant thermal structure has not been studied. This paper analyzes the cloud formation quantitatively. Note that the structure analyzed in this paper is very different from the bow shock and cocoon generated by a supersonically moving object that has a surface (e.g., [Wilkin 1996](#)).

In the next section, we explain our model and the details of our analysis. Results are presented in §3. In §4, we discuss approximate formulates of an interstellar contrail and the possibility of observation. §5 presents a summary. The symbols and their definitions that we use in this paper are compiled in Tab.1.

2. METHODS

2.1. *Orbit of Gas Fragments*

Turbulent structures are ubiquitously observed in the ISM (e.g., [Miville-Deschênes et al. 2016, 2017](#)). To form a linear gaseous structure, it must be formed in a shorter time than eddy turnover time. In this paper we consider a

* Email: kitajima.kanta.z7@s.mail.nagoya-u.ac.jp

Table 1. Notation used in This Paper

Symbol	Definition
A	Particle number accretion rate per unit length of filament
b	Impact parameter
\tilde{b}	Nondimensionalized b with r_{HL}
b_{max}	Impact parameter corresponding to L_{pt}
c_{pre}	Speed of sound in front of the shock wave
$d\dot{M}$	Mass accretion rate per unit length
L	Filament length
L_{pt}	Largest z coordinate where the gas density reaches high enough to be observed by thermal condensation
L'_{pt}	Largest z coordinate where the gas density reaches high enough to be observed by thermal condensation obtained without considering the condition for shock wave generation
L_{sh}	Largest z coordinate where a shock wave is generated
m_{p}	Mass of proton
n_{f}	Number density of gas in the filament
n_{pre}	Number density of gas in front of the shock surface
n_{∞}	Number density of gas in the ambient medium
P_{crit}	Critical pressure of thermal condensation
P_{eq}	Pressure of HI gas in thermal equilibrium
M	Mass of the gravitating object
\dot{M}	Mass accretion rate to the gravitating object
M_{f}	Total mass of filament
\dot{M}_{f}	Mass accretion rate on the filament
\tilde{r}	Radius of a fluid element in units of r_{HL}
r_{HL}	Hoyle–Lyttleton accretion radius
R	Position of filament surface
\tilde{R}	Filament radius in units of r_{HL}
R_{max}	Radius at the end of the filament
s	Position of the stagnation point
T_{eq}	Gas temperature in thermal equilibrium
$T_{\text{post-shock}}$	Gas temperature in the post shock region
v_{FC}	The minimum velocity of a gravitating object to form a contrail
v_z	Velocity component in the filament in the z -axis direction
v_{\perp}	Vertical velocity component at the shock wave front
v_r	Velocity in the r direction
v_{θ}	Velocity in the θ direction
v_{∞}	Velocity of the gravitating object
w	Filament width
z_{f}	The z coordinate of the filament surface
\tilde{z}_{f}	The z coordinate of the filament surface in units of r_{HL}
γ	The ratio of specific heats
Γ	Heating function
Δv	Velocity dispersion inside filament
τ	Filament formation timescale
τ_{d}	Filament dispersal timescale
μ	Mean molecular weight
κ	Density enhancement due to orbital compression
κ_{f}	Density enhancement due to orbital compression at the filament surface
\mathcal{K}_{sh}	Density enhancement by shock compression at the filament surface
Λ	Cooling function
ρ_{∞}	Mass density of the ambient medium

gravitating object moving at supersonic speeds relative to the ISM. For simplicity, we consider the gravitating object moving at a constant velocity through an interstellar gas of uniform density. We describe the hydrodynamical equations in the comoving frame of the gravitating object. In this frame, we expect that the solution is in a steady state. In this section, we neglect the effect of the gas pressure prior to the formation of a shock wave. The effect of the pre-shock pressure will be discussed in §2.3.

2.1.1. Characteristic Length Scale

A characteristic length scale for the accretion onto a gravitating object is called the Hoyle–Lyttleton accretion radius (Hoyle & Lyttleton 1939, 1941; Bondi & Hoyle 1944) and is defined as follows:

$$r_{\text{HL}} = \frac{2GM}{v_{\infty}^2}, \quad (1)$$

where v_{∞} , G , and M are the velocity of the gravitating object, the gravitational constant, and the mass of the gravitating object.

2.1.2. Orbit's Equation

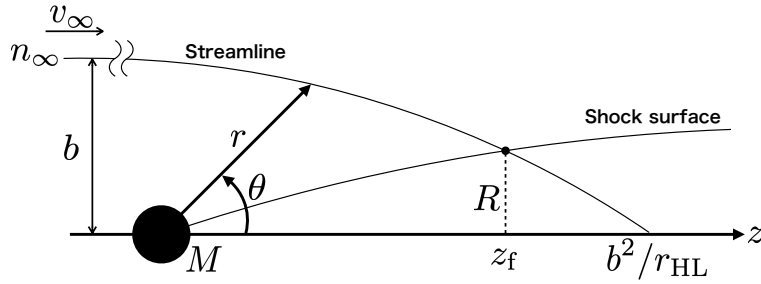


Figure 1. Geometry and sketch.

First, we derive the gas streamline in the rest frame of the gravitating object. Since we are considering uniform background density, the solution should be symmetric with respect to the straight path of the gravitating object. We choose a polar coordinate plane (r, θ, ϕ) , and the resultant structure is uniform in the ϕ direction. If we neglect pressure, gas elements with the same impact parameter intersect at a single point and we choose the z -axis as the line connecting the center of the gravitation object to that point. We consider the geometry shown in Fig.1. If the pressure gradient force can be neglected as described above, the streamline is a freefall solution. The derivation of the orbit of the motion is straightforward (e.g., Binney & Tremaine 2008). Taking the gravitating object as the origin of the coordinates, the gas equation of motion and the boundary condition are given as

$$\ddot{r} - r\dot{\theta}^2 = -\frac{GM}{r^2}, \quad (2)$$

$$\frac{d}{dt}(r^2\dot{\theta}) = 0, \quad (3)$$

$$\lim_{\theta \rightarrow \pi} r \rightarrow \infty, \quad (4)$$

$$\lim_{\theta \rightarrow \pi} \dot{r} \rightarrow -v_{\infty}, \quad (5)$$

and the streamlines are obtained as follows:

$$r = \frac{b^2 v_{\infty}^2}{GM(1 + \cos \theta) + b v_{\infty}^2 \sin \theta}, \quad (6)$$

where b is the impact parameter of the gas fragments. Also, the velocity in the r direction v_r and the θ direction v_{θ} are defined as follows:

$$v_r^2 = \left(1 + \frac{r_{\text{HL}}}{r} - \frac{b^2}{r^2}\right) v_{\infty}^2, \quad (7)$$

$$v_\theta = -r\dot{\theta} = +\frac{b}{r}v_\infty, \quad (8)$$

where $v_r < 0$ for $\theta > \arctan(2b/r_{\text{HL}})$ and $v_r > 0$ for $\theta < \arctan(2b/r_{\text{HL}})$.

Nondimensionalizing the stream equation using r_{HL} yields

$$\tilde{r} = \frac{\tilde{b}^2}{\frac{1}{2}(1 + \cos\theta) + \tilde{b}\sin\theta}, \quad (9)$$

where $\tilde{r} = r/r_{\text{HL}}$ and $\tilde{b} = b/r_{\text{HL}}$. This nondimensional formula is convenient because it does not depend on M or v_∞ .

2.1.3. Compressibility

By the law of conservation of mass and Eq.(6), the compressibility κ due to accretion can be obtained as follows:

$$\kappa = \frac{n}{n_\infty} = \frac{b^2}{r \sin\theta(2b - r \sin\theta)}, \quad (10)$$

where n and n_∞ are the number density at (r, θ) in the streamlines and the number density of the gas far upstream. If the gas falls onto the z -axis, κ will diverge. In reality, the density does not diverge because the shock wave is generated before the gravitationally accelerated gas falls onto the z -axis and the flow is bent to be more in the direction of the z -axis. We define R as the shock surface. From $R = r \sin\theta$, the compressibility on the surface κ_f as follows:

$$\kappa_f = \frac{b^2}{R(2b - R)} = \frac{\tilde{b}^2}{\tilde{R}(2\tilde{b} - \tilde{R})}, \quad (11)$$

where $\tilde{R} = R/r_{\text{HL}}$.

2.1.4. Accretion Rate per Unit Length of the Filament

Now we consider the accretion rate per unit length of the filament. For simplicity, we neglect the shock surface and the filament width. Thereby, the gas falls onto the z -axes and $b^2 = r_{\text{HL}} \cdot z$ holds (substitute $\theta = 0$ in Eq.(6)). In this approximation, the mass accretion rate per unit length $d\dot{M}$ is as follows:

$$d\dot{M} = 2\pi b \cdot db v_\infty \mu m_p n_\infty = \mu m_p A dz, \quad (12)$$

where

$$A = \pi r_{\text{HL}} v_\infty n_\infty. \quad (13)$$

Moreover, μ and m_p are the average molecular weight and the proton mass; $\mu = 1.4$ is used in this study. This equation indicates that the accretion rate on the filament is independent of z .

2.2. Shock Surface

The location of the shock R is estimated from the law of conservation of mass along the z -axis. We assume a steady state for simplicity, the mass conservation law in the z -axis direction is as follows:

$$\frac{\partial}{\partial z}(\pi R^2 n_f v_z) = A, \quad (14)$$

where n_f and v_z are the macroscopic number density inside the shock surface and the velocity along the z -axis. This yields

$$\pi R^2 n_f v_z = A(z - s), \quad (15)$$

where s is a stagnation point. Although it is difficult to determine accurately the location of the stagnation point, it is known to be $s \approx r_{\text{HL}}$ (e.g., Matsuda et al. 2015).

As we are interested in the length of the filament, we seek a solution at $z \gg s$. Since the effect of the gravitating object has almost no effect at $z \gg s$, v_z is the same as v_∞ and then the solution is as follows:

$$\pi R^2 n_f v_\infty = Az. \quad (16)$$

We define the density compression ratio by the shock \mathcal{K}_{sh} . In the limit of a weak shock, the compressibility is close to 1, and in the limit of a strong shock wave, it is 4, so $1 < \mathcal{K}_{\text{sh}} < 4$. Since $n_f = \mathcal{K}_{\text{sh}}\kappa_f n_\infty$ holds, we have

$$R = \sqrt{\frac{r_{\text{HL}}z_f}{\mathcal{K}_{\text{sh}}\kappa_f}}, \quad (17)$$

where z_f is the z value of the intersection of streamline and shock surface.

As in the case of streamlines, the nondimensionalization is as follows:

$$\tilde{R} = \sqrt{\frac{\tilde{z}_f}{\mathcal{K}_{\text{sh}}\kappa_f}}, \quad (18)$$

where $\tilde{z}_f = z_f/r_{\text{HL}}$.

Considering that the shock is not so strong far from the gravitating object and the post-shock region is actually supported by magnetic pressure in the magnetized ISM (e.g., Inoue & Inutsuka 2009), $\mathcal{K}_{\text{sh}} \sim 2.0$ can be used in an approximate calculation.

For the sake of later discussion, we derive the vertical velocity component at the shock wave front v_\perp as follows:

$$v_\perp = - \left. \frac{v_r \left(-\frac{dR(z)}{dz} \cos \theta + \sin \theta \right) - v_\theta \left(\frac{dR(z)}{dz} \sin \theta + \cos \theta \right)}{\sqrt{\left(\frac{dR(z)}{dz} \right)^2 + 1}} \right|_{z=z_f}. \quad (19)$$

2.3. Dimensionless Quantities

By Eqs.(9),(11), and (18), the relation between \tilde{b} and \tilde{z}_f is as follows:

$$\tilde{z}_f^3 + (\tilde{b}^2 - 1)\tilde{z}_f^2 - \mathcal{K}_{\text{sh}}(\mathcal{K}_{\text{sh}} + 2)\tilde{b}^4\tilde{z}_f + \mathcal{K}_{\text{sh}}^2\tilde{b}^6 = 0. \quad (20)$$

The solution is obviously in $0 < z_f < b^2$. As mentioned in §2.2, $\mathcal{K}_{\text{sh}} = 2.0$ is used in this study. From this, we can derive the relationship between dimensionless quantities.

Now, we are interested in the behavior at the point far from the stagnation point. In this case, Eq.(20) is approximated as

$$\tilde{z}_f = \frac{2\mathcal{K}_{\text{sh}}}{\mathcal{K}_{\text{sh}} + 1 + \sqrt{(\mathcal{K}_{\text{sh}} + 1)^2 + 4\mathcal{K}_{\text{sh}}}}\tilde{b}^2. \quad (21)$$

From this equation and $\mathcal{K}_{\text{sh}} = 2.0$, the values of \tilde{z}_f , \tilde{R} , κ_f and v_\perp/v_∞ in the region far from the stagnation point are as follows:

$$\tilde{z}_f \approx 0.562\tilde{b}^2, \quad (22)$$

$$\tilde{R} \approx 0.585\tilde{z}_f^{\frac{1}{2}}, \quad (23)$$

$$\kappa_f \approx 1.46, \quad (24)$$

$$\frac{v_\perp}{v_\infty} \approx 1.04\tilde{z}_f^{-\frac{1}{2}}. \quad (25)$$

From this result, $v_\perp \approx v_\theta(\theta = 0)$ in the region far from the stagnation point (see $v_\theta(\theta = 0)/v_\infty = \tilde{z}^{-1/2}$). Since κ_f does not depend on \tilde{z}_f , the pressure gradient force can be neglected. The calculation results are shown in Fig.2.

2.4. Length of the Filament

2.4.1. Condition of Thermal Condensation

It is known that the evolution of HI gas after the shock compression is almost isobaric and if the post-shock pressure is sufficiently high, the resultant density increases by orders of magnitudes by thermal condensation (Koyama & Inutsuka 2000). In reality, the resultant structure is not a one-phase but a multiphase medium where cold high-density material moves turbulently in a warm low-density medium by the nonlinear development of thermal instability (Koyama & Inutsuka 2002; Audit & Hennebelle 2005; Inoue & Inutsuka 2008, 2009). We expect that such a multiphase medium corresponds to an interstellar contrail. In this study, we assume that if the gas pressure at the post-shock region

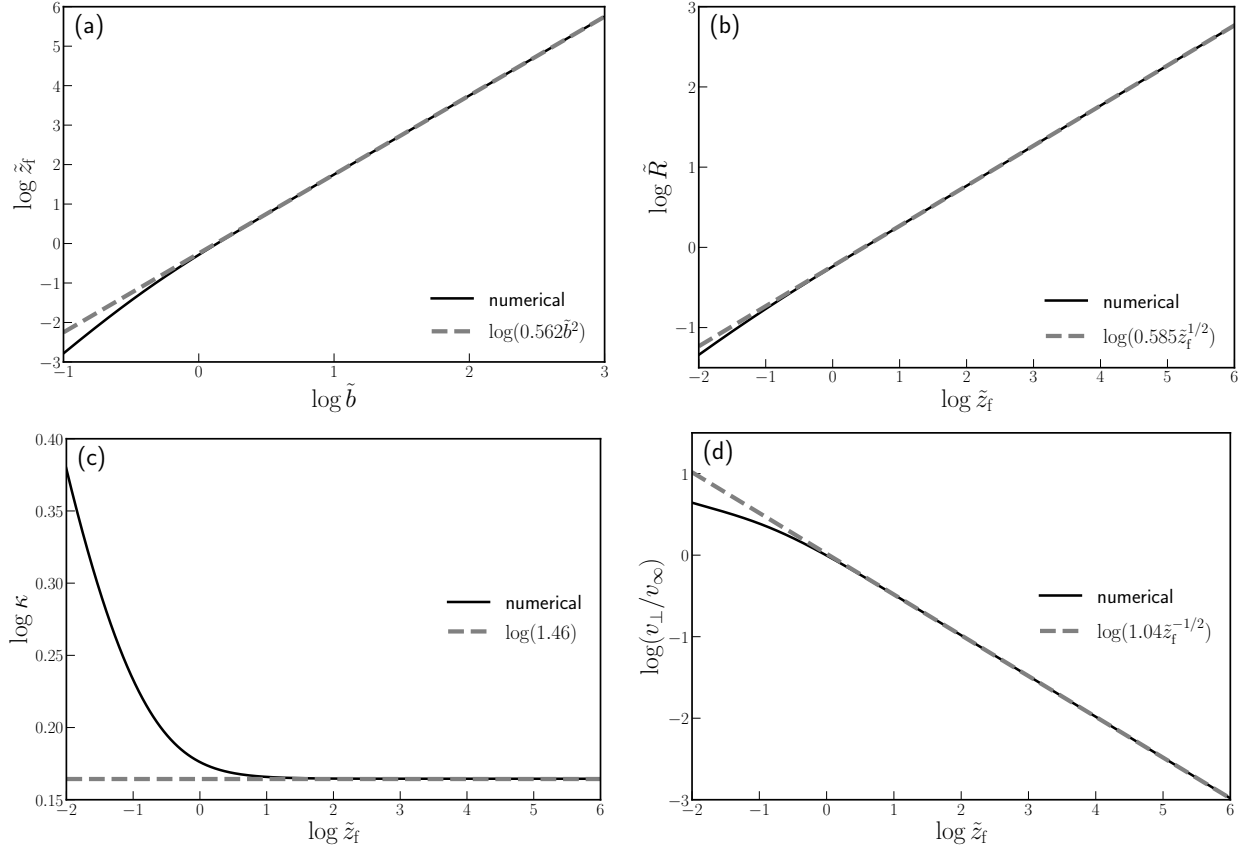


Figure 2. The relationship between dimensionless quantities in the case of $\mathcal{K}_{\text{sh}} = 2.0$. Since the relation $v_z = v_{\infty}$ is used, the behavior before the stagnation point $\tilde{z}_f \lesssim 1$ is different from the real one. The figures show (a) the relationship between the dimensionless impact parameter and the position of the filament on the z -axis $\tilde{z}_f(\tilde{b})$, (b) dimensionless location of the shock surface $\tilde{R}(\tilde{z}_f)$, (c) compressibility on the shock surface $\kappa_f(\tilde{z}_f)$, and (d) dimensionless vertical velocity component at the shock wave front $v_{\perp}(\tilde{z}_f)/v_{\infty}$.

exceeds the critical pressure P_{crit} , the resultant density increases sufficiently to be observed as a filament after thermal condensation. We consider that the filament is observed when its density is 10 times denser than the background gas density, and for the critical pressure P_{crit} , we adopt the following:

$$P_{\text{crit}} = \begin{cases} 10^{3.7} k_{\text{B}} \text{ K cm}^{-3} & (n_{\infty} < 10 \text{ cm}^{-3}), \\ P_{\text{eq}}(n = 10n_{\infty}) & (n_{\infty} \geq 10 \text{ cm}^{-3}), \end{cases} \quad (26)$$

where k_{B} is Boltzmann's constant. $P_{\text{eq}}(n)$ is the pressure of HI gas with a number density of n in thermal equilibrium, which is approximated as

$$\begin{cases} \Gamma = 2 \times 10^{-26} \text{ erg s}^{-1}, \\ \frac{\Lambda(T)}{\Gamma} = 1.0 \times 10^7 \exp\left(\frac{-118400}{T+1000}\right) + 1.4 \times 10^{-2} \sqrt{T} \exp\left(\frac{-92}{T}\right) \text{ cm}^3, \\ -\Gamma + n\Lambda(T = T_{\text{eq}}) = 0, \\ P_{\text{eq}}(n) = nk_{\text{B}}T_{\text{eq}}, \end{cases} \quad (27)$$

where Γ , Λ , T , and T_{eq} are a heating function, a cooling function, the HI gas temperature, and the HI gas temperature in thermal equilibrium (Inoue & Inutsuka 2008). The relation between P_{crit} and P_{eq} is shown in Fig.3.

2.4.2. Critical Distance for Shock Wave Generation

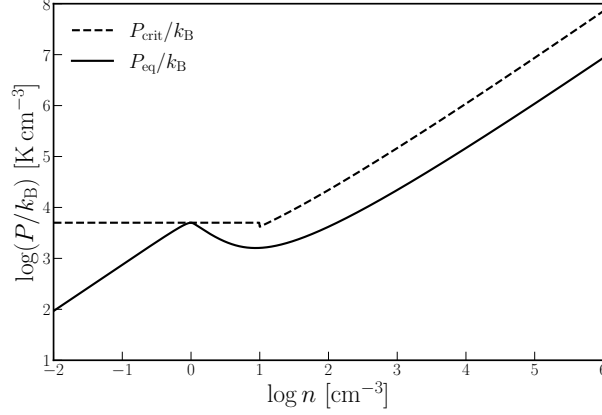


Figure 3. The critical density P_{crit} and the pressure in thermal equilibrium P_{eq} as a function of number density. If the gas pressure increases over P_{crit} by shock, the resultant density grows sufficiently to be observed as a filament after thermal condensation.

We assume that a shock wave is generated if $v_{\perp} > c_{\text{pre}}$; c_{pre} is the speed of sound in front of the shock wave. Assuming that the pre-shock state is in radiative equilibrium, we calculate as follows:

$$c_{\text{pre}}(z_f) = \sqrt{\frac{\gamma k_{\text{B}} T_{\text{eq}}(n_{\text{pre}})}{\mu m_{\text{p}}}}, \quad (28)$$

where $n_{\text{pre}} = \kappa_{\text{f}}(z_{\text{f}})n_{\infty}$, and γ is the specific heat ratio; $\gamma = 5/3$ is used in this study. From these, L_{sh} , the z coordinate of the furthest position where a shock wave is generated, is obtained as

$$v_{\perp}(z_{\text{f}} = L_{\text{sh}}) = c_{\text{pre}}(z_{\text{f}} = L_{\text{sh}}). \quad (29)$$

2.4.3. Length Limit from Thermal Condensation Condition

We estimate the largest z coordinate L_{pt} where the gas density reaches high enough to be observed by thermal condensation. First, assuming a shock wave is generated, we derive the distance from this condition L'_{pt} . The pressure inside the filament P_{f} can be obtained using the momentum conservation law. Because of the angular momentum conservation law, the velocity in the θ direction is very small far from the gravitating object. Assuming that the vertical velocity component in the post-shock region (i.e., in the filament) is negligible and noting that $A = \pi r_{\text{HL}} v_{\infty} n_{\infty}$, the post-shock pressure balances the combination of the ram pressure and pre-shock pressure as

$$P_{\text{f}} = \mu m_{\text{p}} A v_{\perp} \cdot \frac{1}{2\pi R} + P_{\text{pre}} = \frac{1}{2} \rho_{\infty} v_{\infty} v_{\perp} \frac{1}{R} + P_{\text{pre}}, \quad (30)$$

where $\rho_{\infty} = \mu m_{\text{p}} n_{\infty}$ and P_{pre} is the pressure at the shock wave front.

Assuming thermal equilibrium conditions, P_{pre} is as follows:

$$P_{\text{pre}} = P_{\text{eq}}(n_{\text{pre}}). \quad (31)$$

L'_{pt} is obtained from the following relation:

$$P_{\text{f}}(z_{\text{f}} = L'_{\text{pt}}) = P_{\text{crit}}. \quad (32)$$

From these, L_{pt} is obtained from the following relation:

$$L_{\text{pt}} = \min(L'_{\text{pt}}, L_{\text{sh}}). \quad (33)$$

Although we adopt a thermal radiative equilibrium value for the pre-shock temperature in Eq.(28) and pressure in Eq.(31), the resulting value of L_{pt} does not change much even if we adopt the pressure value of adiabatic compression. This is because $\kappa_{\text{f}} \approx 1.46$ is not very large.

2.4.4. Filament Length

If gases become thermally unstable by shock compression, they grow into a mixture of CNM and WNM in a turbulent state (Koyama & Inutsuka 2002). In this study, we model the resultant shocked gas flowing in the z -axis direction as a multiphase filamentary structure that will diffuse out in the region far away from the gravitating object.

We estimate the dispersal timescale τ_d . After the shock compression, a fraction of the gas becomes a cold dense phase by thermal instability, but the low-density warm gas tends to be supported by the interstellar magnetic field. As a result, the average density does not increase much. Thus, we approximately use n_f as the overall macroscopic number density of the gas after the shock compression. We assume that the gas expands by turbulence while flowing at v_∞ in the z -axis direction and we define the dispersal time at which the overall decreasing density reaches n_∞ . From the law of conservation of mass, the following equation is obtained:

$$\pi R^2(L_{\text{pt}})n_f = \pi R_{\text{max}}^2 n_\infty, \quad (34)$$

where R_{max} is the radius at the end of the filament. From this, τ_d can be estimated as follows:

$$\tau_d = \frac{R_{\text{max}} - R(L_{\text{pt}})}{\Delta v}, \quad (35)$$

where Δv is the dispersion velocity inside the filament, and we estimate as follows:

$$\Delta v = \sqrt{\frac{\gamma k_B T_{\text{post-shock}}}{\mu m_p}}, \quad (36)$$

where $T_{\text{post-shock}}$ is the temperature in thermal equilibrium in the post-shock region, and $T_{\text{post-shock}} = T_{\text{eq}}(n_f(L_{\text{pt}}))$. Using the dispersal time scale we define the filament length in the following:

$$L = L_{\text{pt}} + \tau_d v_\infty. \quad (37)$$

2.5. Basic Dimensions of the Filament

We estimate other basic dimensions of the filament such as the width and the total mass. Since the filament boundary surface depends on the value of z , a representative value is taken as the filament width. This study estimates the filament width w as follows:

$$w = 2R(L_{\text{pt}}). \quad (38)$$

Next, we approximate the total filament mass M_f . We denote $b_{\text{max}} = b(L_{\text{pt}})$, and the accretion rate on the filament \dot{M}_f is as follows:

$$\dot{M}_f = \pi b_{\text{max}}^2 \rho_\infty v_\infty. \quad (39)$$

Since the filament formation timescale $\tau = L/v_\infty$, M_f is obtained as follows:

$$M_f = \dot{M}_f \tau = \pi b_{\text{max}}^2 \rho_\infty L. \quad (40)$$

3. OVERALL RESULT

We calculate the length L , the width w , b_{max} and the total mass M_f from with $M = 1, 10^4 M_\odot$, $v_\infty = 20, 200 \text{ km s}^{-1}$, and $10^{-2} \text{ cm}^{-3} \leq n_\infty \leq 10^6 \text{ cm}^{-3}$. We consider a stellar-mass and an intermediate-mass black hole as a gravitating object. For the velocity of those objects relative to the ambient ISM, we consider the range from the speed of sound of WNM ($\sim 10 \text{ km s}^{-1}$) and the virial velocity in our galaxy ($\sim \text{a few } 10^2 \text{ km s}^{-1}$). The background gas is assumed to be WNM or CNM. A range of densities including WNM and CNM was employed as the density of the background gas (e.g., Cox 2005; Hennebelle & Inutsuka 2019). Fig.4 shows the result of the calculation. We find that various filaments are formed depending on the parameters such as mass and velocity of the gravitating object, and background density. Especially notable is that a compact object more massive than $10^4 M_\odot$ can make a filament whose length is larger than 100 pc.

This section describes the qualitative behavior. Quantitative estimates are provided in §4.1.

The length is an increasing function of M and n_∞ as shown in Fig.4(a) because the momentum flux increases with M and n_∞ as can be seen in Eq.(13). Moreover, the filament length does not depend on v_∞ if v_∞ is sufficiently large

($v_\infty > v_{\text{FC}}$; v_{FC} will be discussed in §4.2) because for increasing v_∞ , the effect of increasing the momentum flux and decreasing the mass accretion rate per unit length A (see Eqs.(1) and (13)) cancel each other. The filament width w is an increasing function of M and n_∞ and decreasing function of v_∞ as shown in Fig.4(b). The reason for an increasing function of M and n_∞ is the same as the reason for the length's behavior (see Eq.(38)). The reason for the filament width is a decreasing function of v_∞ where the total mass M_f becomes smaller as v_∞ becomes larger as will be explained later and the filament length does not depend on v_∞ .

The impact parameter b_{max} that corresponds to L_{pt} is also an increasing function of M and n_∞ and decreasing function of v_∞ as shown in Fig.4(c). The reason for an increasing function of M and n_∞ is the same as the reason for the length's behavior. The reason for the decreasing function of v_∞ is derived from r_{HL} , which is also a decreasing function of v_∞ and $b^2 = r_{\text{HL}} \cdot z$ holds (substitute $\theta = 0$ in Eq.(6)).

The total filament mass M_f is also an increasing function of M and n_∞ and decreasing function of v_∞ as shown in Fig.4(d). The reason for this behavior can be understood from the behavior of b_{max} and L (see Eq.(40)). The reason for this behavior can also be understood as follows. If v_∞ is larger, the filament formation timescale τ is shorter and the accretion rate on the filament \dot{M}_f is also small.

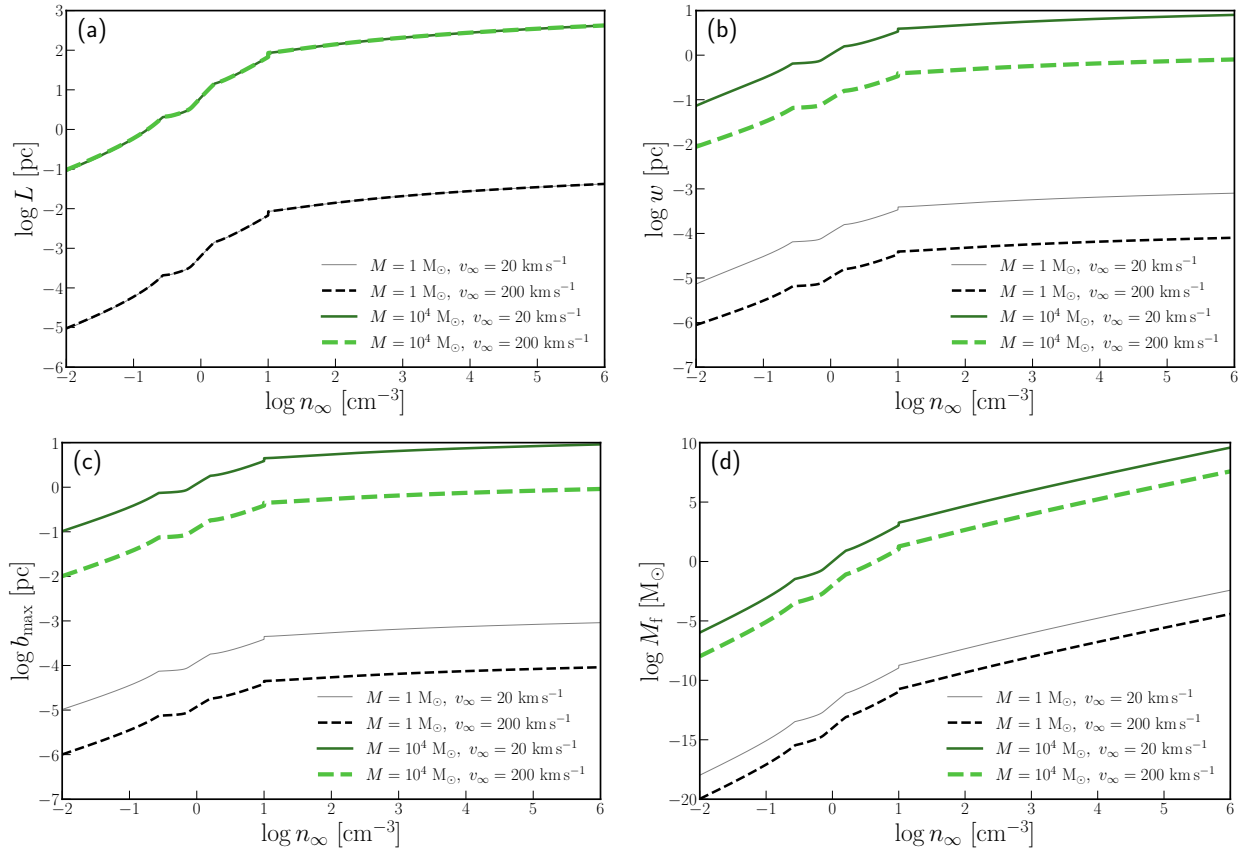


Figure 4. The basic dimensions of the filament. The figures show (a) length L , (b) width w , (c) b_{max} , and (d) total mass M_f .

4. DISCUSSION

4.1. Approximate Expressions for Various Physical Quantities of the Filaments

We derive expressions for various physical quantities of filaments. For simplicity, we ignore P_{pre} and use the approximation $L \approx 2L'_{\text{pt}}$. In this approximation, the length L follows from Eqs.(23), (25), (30), and (32) so that

$$L \approx 2.59 \text{ pc} \left(\frac{M}{10^4 M_\odot} \right) \left(\frac{n_\infty}{0.5 \text{ cm}^{-3}} \right) \left(\frac{P_{\text{crit}}/k_B}{10^{3.7} \text{ K cm}^{-3}} \right)^{-1}. \quad (41)$$

Thus, it is shown that L does not depend on v_∞ .

Using the approximation $L_{\text{pt}} \approx L'_{\text{pt}}$, the filament width w , b_{max} and total mass M_f can be estimated similarly as follows:

$$w \approx 6.17 \times 10^{-2} \text{ pc} \left(\frac{M}{10^4 M_\odot} \right) \left(\frac{v_\infty}{200 \text{ km s}^{-1}} \right)^{-1} \left(\frac{n_\infty}{0.5 \text{ cm}^{-3}} \right)^{1/2} \left(\frac{P_{\text{crit}}/k_B}{10^{3.7} \text{ K cm}^{-3}} \right)^{-1/2}, \quad (42)$$

$$b_{\text{max}} \approx 7.03 \times 10^{-2} \text{ pc} \left(\frac{M}{10^4 M_\odot} \right) \left(\frac{v_\infty}{200 \text{ km s}^{-1}} \right)^{-1} \left(\frac{n_\infty}{0.5 \text{ cm}^{-3}} \right)^{1/2} \left(\frac{P_{\text{crit}}/k_B}{10^{3.7} \text{ K cm}^{-3}} \right)^{-1/2}, \quad (43)$$

$$M_f \approx 6.96 \times 10^{-4} M_\odot \left(\frac{M}{10^4 M_\odot} \right)^3 \left(\frac{v_\infty}{200 \text{ km s}^{-1}} \right)^{-2} \left(\frac{n_\infty}{0.5 \text{ cm}^{-3}} \right)^3 \left(\frac{P_{\text{crit}}/k_B}{10^{3.7} \text{ K cm}^{-3}} \right)^{-2}. \quad (44)$$

4.2. Conditions for Contrail Formation

First, the radius of the gravitating object should be much larger than b_{max} for creating a contrail. Second, if a massive compact object moves at a very low velocity, the object only absorbs surrounding gases and obviously does not create a contrail. In such situations, the stagnation point ($s \approx r_{\text{HL}}$) is located far away from the massive object in our framework and the gravitational focusing is negligible. If the relative speed v_∞ satisfies $L_{\text{pt}} > r_{\text{HL}}$, the interstellar contrail is expected to form. We denote such condition by $v_\infty > v_{\text{FC}}$ where v_{FC} is estimated from the approximation $L_{\text{pt}} \approx L'_{\text{pt}}$ as follows:

$$v_{\text{FC}} \approx 8.15 \text{ km s}^{-1} \left(\frac{n_\infty}{0.5 \text{ cm}^{-3}} \right)^{-1/2} \left(\frac{P_{\text{crit}}/k_B}{10^{3.7} \text{ K cm}^{-3}} \right)^{1/2}. \quad (45)$$

The ratio of L_{pt} and r_{HL} is shown in Fig.5.

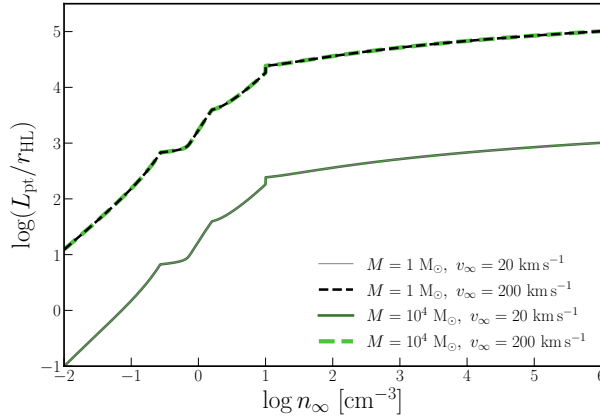


Figure 5. The ratio of L_{pt} and r_{HL} . This figure shows that the slower the gravitating object moves, the farther the stagnation point is located from the object. If $\log(L_{\text{pt}}/r_{\text{HL}}) > 0$, we expect that filament should be formed.

4.3. Filament Formation Site

The Galactic midplane is supposed to be occupied mostly by WNM except in bubbles due to supernova explosions. The estimation in §4.1 corresponds to the case when a massive compact object moves in WNM. This process is very different from the formation of filamentary molecular clouds in a shock-compressed layer (e.g., Abe et al. 2021).

On the other hand, a limited volume of the Galactic disk corresponds to CNM (i.e., cold HI clouds and molecular clouds). If the CNM size is large enough, a massive object of $10^4 M_\odot$ may create a long filament as large as 100 pc, which should be compared to those observed in Zucker et al. (2018). If the CNM size is smaller than $2b_{\text{max}}$, the filament length is smaller than that estimated in this study. If the CNM is distributed intermittently on the trajectory of the gravitating source, the resulting filament might have spatially disconnected (see Fig.6).

Recent 21 cm line observations (e.g., HI4PI Collaboration et al. 2016) have revealed the existence of numerous linear structures along the interstellar magnetic fields in HI clouds (e.g., Clark et al. 2014; Jelić et al. 2018; Turic et al. 2021). It is difficult to determine the distance to those filaments, which is one of the difficulties in understanding

their property. Although such filamentary structures seem to be ubiquitous on the celestial plane, the cause of those structures is not fully understood. Thus, it is interesting to consider the possibility of creating filamentary structures by multiple gravitating sources passing through the shell of the Local Bubble. The typical length of observed HI filaments is roughly estimated as 1–10 pc if they are located on the surface of the Local Bubble whose radius is about 50 pc (e.g., Zucker et al. 2022). With Eqs. (41) – (44) we can estimate the condition for a gravitating object to form these filaments. For example, we consider a gravitating object passing through the Local Bubble’s shell. If the number density of ambient gas is 20 cm^{-3} , gravitating objects of 10 , 10^2 , and $10^3 M_\odot$ create filaments with lengths of approximately 0.078, 0.78, and 7.8 pc, respectively. Whereas the number density is 200 cm^{-3} , gravitating objects of 10 , 10^2 , and $10^3 M_\odot$ create approximately 0.14, 1.4, and 14 pc, respectively. Note that P_{crit} is not a simple linear function of n_∞ so the filament length (Eq. (41)) has a nonlinear dependence on n_∞ . We should note, however, that the thermal condensation is hindered by the interstellar magnetic field (e.g., Inoue & Inutsuka 2008, 2009), and the length of the interstellar contrail becomes shorter than our model if the strength of the magnetic field is significantly large. It is difficult to treat the effects of magnetic fields in the present analytical framework and we will study them by numerical simulation in the future.

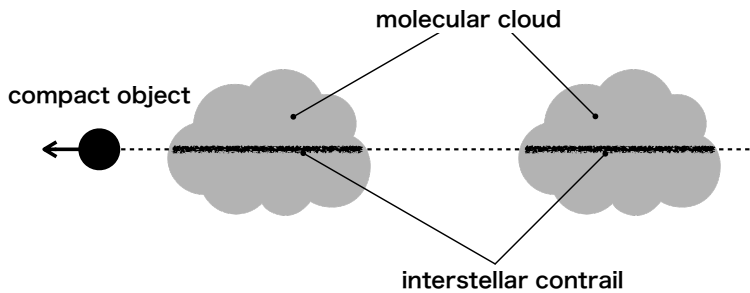


Figure 6. Almost straight but spatially disconnected filaments can be formed by this model. The dashed line denotes the pathway of the compact object.

4.4. Accretion to Gravitating Source

Accretion onto a moving gravitating source is called Bondi–Hoyle–Lyttleton accretion (Hoyle & Lyttleton 1939, 1941; Bondi & Hoyle 1944), and the mass accretion rate to the gravitating source can be estimated by

$$\dot{M} = \pi r_{\text{HL}}^2 \rho_\infty v_\infty \quad (46)$$

$$\approx 5.13 \times 10^{-11} M_\odot \text{ yr}^{-1} \left(\frac{M}{10^4 M_\odot} \right)^2 \left(\frac{v_\infty}{200 \text{ km s}^{-1}} \right)^{-3} \left(\frac{n_\infty}{0.5 \text{ cm}^{-3}} \right). \quad (47)$$

This value seems to be too small to be observed. A detailed discussion on observability is beyond the scope of this paper (see, e.g., Fukue & Ioroi 1999; Ogata et al. 2021).

5. CONCLUSIONS

We propose a new mechanism for creating an interstellar contrail formed by the thermal condensation of HI gas or molecular gas in the trajectory of a fast-moving gravitating source in the ISM, and estimate the characteristics of the interstellar contrail analytically. The results show that the filament length is independent of the relative velocity of the gas and the gravitating object if the formation conditions are satisfied. It is also found that filaments with a variety of lengths, widths, and masses can be formed depending on the mass of the gravitating source, relative velocity, and the density of ambient gas. The resulting filament is expected to be in thermal equilibrium and the average number density depends on P_{crit} . Roughly speaking, if the gravitating object passes through in WNM, the number density of the filament is on the order of 100 cm^{-3} and if the gravitating object passes through in the dense region such as CNM or molecular cloud, the number density of the filament is about 1000 cm^{-3} or more. For example, when a $10^2 M_\odot$ object passes through the dense region ($n_\infty \sim 200 \text{ cm}^{-3}$) in the shell of the Local Bubble, it creates a filament whose length is about 1.4 pc. In particular, if a compact object more massive than $10^4 M_\odot$ such as an intermediate-mass black hole goes through a large region of mostly cold atomic or molecular gas, it can form a filament whose length is

larger than a hundred parsecs. If we observationally identify such phenomena in multiple regions, we will be able to estimate the frequency of intermediate-mass black holes that are not luminous enough to be visible. This line of work is expected to provide an important step toward understanding the formation process of massive black holes.

This work was financially supported by JST SPRING, Grant Number JPMJSP2125. The author (K.K.) would like to take this opportunity to thank the “Interdisciplinary Frontier Next-Generation Researcher Program of the Tokai Higher Education and Research System. The author (S.I.) is supported by JSPS Grants-in-Aid for Scientific Research Nos. 16H02160, 18H05436, and 18H05437. We thank the anonymous referee for constructive comments. We also thank J. Shimoda for the useful discussion.

REFERENCES

- Abe, D., Inoue, T., Inutsuka, S.-i., & Matsumoto, T. 2021, *ApJ*, 916, 83, doi: [10.3847/1538-4357/ac07a1](https://doi.org/10.3847/1538-4357/ac07a1)
- Audit, E., & Hennebelle, P. 2005, *A&A*, 433, 1, doi: [10.1051/0004-6361:20041474](https://doi.org/10.1051/0004-6361:20041474)
- Binney, J., & Tremaine, S. 2008, *Galactic Dynamics: Second Edition* (Princeton University Press)
- Bondi, H., & Hoyle, F. 1944, *MNRAS*, 104, 273, doi: [10.1093/mnras/104.5.273](https://doi.org/10.1093/mnras/104.5.273)
- Clark, S. E., Peek, J. E. G., & Putman, M. E. 2014, *ApJ*, 789, 82, doi: [10.1088/0004-637X/789/1/82](https://doi.org/10.1088/0004-637X/789/1/82)
- Cox, D. P. 2005, *ARA&A*, 43, 337, doi: [10.1146/annurev.astro.43.072103.150615](https://doi.org/10.1146/annurev.astro.43.072103.150615)
- Falle, S. A. E. G., Wareing, C. J., & Pittard, J. M. 2020, *MNRAS*, 492, 4484, doi: [10.1093/mnras/staa131](https://doi.org/10.1093/mnras/staa131)
- Ferrière, K. 1998, *ApJ*, 497, 759, doi: [10.1086/305469](https://doi.org/10.1086/305469)
- Field, G. B. 1965, *ApJ*, 142, 531, doi: [10.1086/148317](https://doi.org/10.1086/148317)
- Field, G. B., Goldsmith, D. W., & Habing, H. J. 1969, *ApJL*, 155, L149, doi: [10.1086/180324](https://doi.org/10.1086/180324)
- Fukue, J., & Ioroi, M. 1999, *PASJ*, 51, 151, doi: [10.1093/pasj/51.1.151](https://doi.org/10.1093/pasj/51.1.151)
- Hennebelle, P., & Inutsuka, S.-i. 2019, *Frontiers in Astronomy and Space Sciences*, 6, 5, doi: [10.3389/fspas.2019.00005](https://doi.org/10.3389/fspas.2019.00005)
- HI4PI Collaboration, Ben Bekhti, N., Flöer, L., et al. 2016, *A&A*, 594, A116, doi: [10.1051/0004-6361/201629178](https://doi.org/10.1051/0004-6361/201629178)
- Hoyle, F., & Lyttleton, R. A. 1939, *Proceedings of the Cambridge Philosophical Society*, 35, 405, doi: [10.1017/S0305004100021150](https://doi.org/10.1017/S0305004100021150)
- . 1941, *MNRAS*, 101, 227, doi: [10.1093/mnras/101.4.227](https://doi.org/10.1093/mnras/101.4.227)
- Inoue, T., & Inutsuka, S.-i. 2008, *ApJ*, 687, 303, doi: [10.1086/590528](https://doi.org/10.1086/590528)
- . 2009, *ApJ*, 704, 161, doi: [10.1088/0004-637X/704/1/161](https://doi.org/10.1088/0004-637X/704/1/161)
- Jelić, V., Prelogović, D., Haverkorn, M., Remeijn, J., & Klindžić, D. 2018, *A&A*, 615, L3, doi: [10.1051/0004-6361/201833291](https://doi.org/10.1051/0004-6361/201833291)
- Koyama, H., & Inutsuka, S.-I. 2000, *ApJ*, 532, 980, doi: [10.1086/308594](https://doi.org/10.1086/308594)
- Koyama, H., & Inutsuka, S.-i. 2002, *ApJL*, 564, L97, doi: [10.1086/338978](https://doi.org/10.1086/338978)
- Kupilas, M. M., Wareing, C. J., Pittard, J. M., & Falle, S. A. E. G. 2021, *MNRAS*, 501, 3137, doi: [10.1093/mnras/staa3889](https://doi.org/10.1093/mnras/staa3889)
- Li, G.-X., & Shi, X. 2021, *MNRAS*, 503, 4466, doi: [10.1093/mnras/stab735](https://doi.org/10.1093/mnras/stab735)
- Martinez-Medina, L. A., Pichardo, B., Moreno, E., Peimbert, A., & Velazquez, H. 2016, *ApJL*, 817, L3, doi: [10.3847/2041-8205/817/1/L3](https://doi.org/10.3847/2041-8205/817/1/L3)
- Matsuda, T., Isaka, H., & Ohsugi, Y. 2015, *Progress of Theoretical and Experimental Physics*, 2015, 113E01, doi: [10.1093/ptep/ptv148](https://doi.org/10.1093/ptep/ptv148)
- Miville-Deschênes, M. A., Duc, P. A., Marleau, F., et al. 2016, *A&A*, 593, A4, doi: [10.1051/0004-6361/201628503](https://doi.org/10.1051/0004-6361/201628503)
- Miville-Deschênes, M.-A., Murray, N., & Lee, E. J. 2017, *ApJ*, 834, 57, doi: [10.3847/1538-4357/834/1/57](https://doi.org/10.3847/1538-4357/834/1/57)
- Ogata, E., Ohsuga, K., & Yajima, H. 2021, *PASJ*, 73, 929, doi: [10.1093/pasj/psab055](https://doi.org/10.1093/pasj/psab055)
- Turić, L., Jelić, V., Jaspers, R., et al. 2021, *A&A*, 654, A5, doi: [10.1051/0004-6361/202141071](https://doi.org/10.1051/0004-6361/202141071)
- Wallin, J. F., Higdon, J. L., & Staveley-Smith, L. 1996, *ApJ*, 459, 555, doi: [10.1086/176920](https://doi.org/10.1086/176920)
- Wilkin, F. P. 1996, *ApJL*, 459, L31, doi: [10.1086/309939](https://doi.org/10.1086/309939)
- Zucker, C., Battersby, C., & Goodman, A. 2018, *ApJ*, 864, 153, doi: [10.3847/1538-4357/aacc66](https://doi.org/10.3847/1538-4357/aacc66)
- Zucker, C., Goodman, A. A., Alves, J., et al. 2022, *Nature*, 601, 334, doi: [10.1038/s41586-021-04286-5](https://doi.org/10.1038/s41586-021-04286-5)